

Understanding global teleconnections to surface air temperatures in Japan based on a new climate classification

Pascal Oettli¹  | Masami Nonaka¹ | Masahiko Kuroki² | Hiroyuki Koshiba² | Yosuke Tokiya² | Swadhin K. Behera¹

¹Research Institute for Value-Added-Information Generation Application Laboratory (VAiG APL), Japan Agency for Marine-Earth Science and Technology (JAMSTEC), Yokohama, Japan

²JERA (Japan Energy Era) Co., Inc., Tokyo, Japan

Correspondence

Pascal Oettli, 3173-25, Showa-machi, Kanazawa-ku, Yokohama City, Kanagawa 236-0001, Japan.
Email: oettli@jamstec.go.jp

Funding information

JERA Co., Inc.

Abstract

Utilizing the self-organizing map (SOM), a type of artificial neural network, a new classification of the climate of Japan is proposed. The SOM is applied on the monthly mean surface air temperature (SAT) anomalies, extracted from 762 stations. Considering the strong seasonal cycle in mid-latitudes, the classification is performed for two distinct seasons, boreal winter and boreal summer. Applied on monthly average temperature, to capture the seasonal signal, the SOM is an easily implementable interesting tool to (a) objectively capture the patterns present in the input data, and (b) identify the source of inter-annual variability, which is crucial for power demand forecasting. While modulated by local conditions, SAT in Japan is mainly influenced by large-scale circulation. It is found in this study that stronger relationships exist for tropics with southern regions and for extra-tropics with northern regions, in the seasonally oriented teleconnection patterns. In winter, the regions are organized along a north–south orientation, with a secondary west–east orientation in the central part of the country. This organization is a function of the strength of the link with the tropical Pacific and Indian Oceans sea-surface temperatures. Changes in the speed of the westerly jet, together with the modulation of the Western Pacific (WP)-like and Eurasian (EU)-like patterns, are also important for SAT in Japan in winter. In summer, the main organization follows a west–east orientation. The Pacific Japan (PJ)-like pattern plays an important role in the geographical distribution of the SAT, together with the existence of mid-latitude and subtropical wave trains, like the Silk Road (SR)-like pattern.

KEY WORDS

climate classification, interannual variability, Japan, teleconnection

1 | INTRODUCTION

Climate classification is a way to simplify the complexity of the Earth's climate system, identifying similar features and defining spatial boundaries (Oliver, 2005). Among

the many ways to classify the climates (for a more complete list see Oliver, 2005), the Köppen system, constructed on the basis of vegetation groups and on the annual and seasonal temperature and precipitation (Köppen, 1900, 1918; Geiger, 1954), is certainly the most

widely known and the most frequently used classification (Kottek *et al.*, 2006). Utilizing the moisture balance, Thornthwaite (1931, 1948) introduced another way to classify the world's climates, considering the precipitation effectiveness and the thermal efficiency. Similar techniques are sometime used to classify regional climate.

However, heuristic approach of the climate classification has inherent limitations. Thornthwaite (1943) pointed out the lack of process understanding during the process of classification and the problem of the definition of boundaries. Later, Willmott (1977) also stressed the need to address the arbitrary decisions about what constitutes a climatic boundary.

Data driven approaches is a way to address issues linked to heuristic approach, by investigating the inherent patterns in multiple data streams (Zscheischler *et al.*, 2012). The first such attempts to use numerical classification were made by Steiner (1960) to divide the conterminous United States into 10 climatic regions, combining a factor analysis and a hierarchical cluster analysis. Similar works are seen at country scales for Nigeria (Ayoade, 1976), Australia (McBoyle, 1971), and South-Africa (Preston-Whyte, 1974). It was also applied at continental scale (McBoyle, 1972; Anyadike, 1987) as well as global scales (Cannon, 2012; Zscheischler *et al.*, 2012).

For Japan, the first published climatic division was proposed by Nakagawa (1899). Considering temperature, precipitation, wind and land features, Japan was divided into nine regions. Following this work, many studies have been published, presenting different divisions of the Japanese climate (e.g., Mizukoshi, 1977). Also, the conventional classification methods, that is, Köppen's (Fukui, 1938; Sekiguchi, 1949) and Thornthwaite's (Isozaki, 1933; Fukui, 1957), as well as data-driven methods have been applied to Japan. Sekiguchi (1959) calculated correlations between each station and its neighbouring stations with diurnal range of air temperature, number of rainy days, percentage of possible sunshine, and amount of water surplus to divide Japanese climate into 6 regions and 18 sub-regions (with 8 transitional zones). Focusing on the Tohoku district, Kojima (1973) used principal component analysis (PCA) for a detailed climatic classification, defining 21 small climatic areas, united into 9 zones. Combining PCA and cluster analysis, Koizumi and Kato (2012) defined 14 climatic zones and transitional zones covering the whole country.

These studies generally used k-means (MacQueen, 1967), an unsupervised and nonhierarchical clustering approach, which associates objects to the nearest centroid by multiple iterations, by minimizing the within-cluster variances (Lloyd, 1957; Forgy, 1965; Hartigan and Wong, 1979) and relocating misplaced objects (Wilks, 2011). However, k-means is sensitive to the noise and outliers

can affect the calculation of cluster centre. PCA (Pearson, 1901; Hotelling, 1936) is a dimensionality reduction technique. In meteorology, PCA is largely utilized to analyse the variability of a single field (Björnsson and Venegas, 1997), finding spatial patterns of variability and their variation in time (Preisendorfer, 1988). Nevertheless, PCA also has some shortcomings due to linear assumptions and linear transformation. This may lead to the extraction of artificial patterns, never realized in input data or to the extraction of patterns with no physical meaning, while still under debate (Dommenget and Latif, 2002, 2003; Behera *et al.*, 2003; Jolliffe, 2003; Hannachi *et al.*, 2006).

To overcome the sensitivity to outliers and to preserve the topology of the data, the self-organizing map (SOM) became a popular algorithm among climatologists and meteorologists (e.g. Hewitson and Crane, 2002; Leloup *et al.*, 2007, 2008; Tozuka *et al.*, 2008; Morioka *et al.*, 2010; Liu and Weisberg, 2011; Chattopadhyay *et al.*, 2013; Oettli *et al.*, 2014; Wolski *et al.*, 2018), with remarkable success. SOM is a type of artificial neural network, with an unsupervised learning for the training (Kohonen, 1982, 2001). This algorithm produces an array of nonlinear low-dimensional output ("nodes"), usually two-dimensional, from a high-dimensional, varying in time, input data (Ohba *et al.*, 2016). In climate application, the nodes can be represented as an array of idealized, spatially organized, maps of the targeted variable (Ohba *et al.*, 2016; Wolski *et al.*, 2018). With an appropriate size, SOM accurately captures both the patterns present in the input data and their relative occurrence frequencies (Reusch *et al.*, 2005; Liu *et al.*, 2006; Annas *et al.*, 2007; Astel *et al.*, 2007). Moreover, SOM preserves the topology of the patterns.

Considering its utility and reliability, we use SOM technique for the classification of the Japanese climate in this study. Power demand forecasting few months ahead is important. In Japan, a strong correlation exists between summer and winter temperatures and the electric power demand. In regard to this matter, identification of surface air temperature (SAT)-based climate regions and the sources of variability in the regions is crucial for power demand forecasting few months ahead. To achieve this, we explore the relationship between regional SAT derived from the classification and global fields.

We discuss the results of the classification after introducing the data and the methods. By its location, Japan has different types of climate, ranging from subarctic in the north to subtropical in the south. Between the Pacific side and the Sea of Japan side, conditions are also different. To consider the strong seasonal cycle in mid-latitudes, the classification is performed on the monthly mean SAT of two seasons, that is, boreal winter

(December–January–February, hereinafter DJF) and boreal summer (June–July–August, hereinafter JJA). Because SAT is influenced by both local conditions and large-scale circulation, it is a useful data to discriminate regions, considering similarity/difference in the response to local and remote forcing.

Data and methods are first described in Section 2. Then results of the SOM are detailed and the relations with different global fields are explored, first for boreal winter in Section 3, then for boreal summer in Section 4. Finally, results are summarized in Section 5 and discussed in Section 6.

2 | DATA AND METHODS

From the AMeDAS (Automated Meteorological Data Acquisition System) network maintained by the Japanese Meteorological Agency (JMA, 2018), monthly mean SAT of 762 stations is extracted (Figure 1a), for the period 1980–2017. This selection is meant to cover all the types of climate. Except the initial quality check performed at JMA, no further quality check has been done, as well as any homogenization has been performed before the analyses. Departure from the monthly climatology (1981–2010) is calculated and interannual signal is isolated by a bandpass wavelet filter (Torrence and Compo, 1998), keeping only the variability between 3 months (beyond the synoptic and intraseasonal time scales) and 8 years (behind decadal and multidecadal time scales). Filtering is performed to improve the detection of large-scale teleconnection patterns, likely to cause the variation of regional SAT on interannual scale, that is, the scale of interest in the present study. From filtered anomalies, the data for two seasons are retrieved: one subset for DJF (114 months) and another subset for JJA (114 months). For consistency, all other variables presented below have been filtered and subsetted following the same process.

The Met Office Hadley Centre's sea ice and sea surface temperatures HadISST (Rayner *et al.*, 2003) are used. The zonal and meridional components of the wind (respectively, U and V) are extracted from the NCEP–DOE AMIP-II Reanalysis NCEP2 (Kanamitsu *et al.*, 2002) at three different pressure levels (850, 500, and 300 hPa). Outgoing longwave radiation (OLR) from the NOAA Climate Data Record Program (Lee and NOAA CDR Program, 2018) is used as a proxy of the convective activity inside the tropical band and of the cloud cover outside. The West Pacific index is retrieved from the NOAA Climate Prediction Center website (ftp://ftp.cpc.ncep.noaa.gov/wd52dg/data/indices/wp_index.tim) and the Eurasian index is calculated following the definition given by Wallace and Gutzler (1981).

Concurrence of SAT and global variables cited previously is explored with the help of correlation coefficients, with no time lag (i.e., simultaneous correlation). The significance of the correlations is tested via Monte Carlo resampling (Strasser and Weber, 1999; Hothorn *et al.*, 2006), with 10,000 replicates and the *p*-value significance is 0.05. All calculations and graphics are made using the R project for statistical computing version 3.5.1 (R Core Team, 2018, <https://www.r-project.org/>), with the help of packages “coin” version 1.2–2 (Hothorn *et al.*, 2008), “kohonen” verion 3.0.7 (Wehrens and Buydens, 2007; Wehrens and Kruisselbrink, 2018) and “WGCNA” version 1.67 (Langfelder and Horvath, 2008, 2012) for calculations, “ggplot2” version 3.3.1 (Wickham, 2016) and “metR” version 0.2.0 (<https://github.com/eliocamp/metR/>) for graphics.

Climate classification is done via the application of the SOM algorithms to the SAT data. SOM is run on each season, that is, on a matrix of 762 stations by 114 months. Readers can refer to Tozuka *et al.* (2008) and Morioka *et al.* (2010) for the detailed procedure.

To avoid over-clustering, the total number of nodes must be limited, but at the same time, a lower number of nodes could deplete the signal in teleconnections though broadly improve the representation of the analysed regions. After several trials, we found the rectangular size 4 × 2 (i.e., 8 nodes) provides the clearer signal in teleconnections as well as maintaining the regionalization of SAT for each season. As a result, 762 stations are classified into eight regions (Figure 1).

By construction, SAT indices might have significant correlation. However, for several years (i.e., 1988, 1997–2001, 2003, 2013, and so forth), differences in anomalies are large, as seen in Figure 1c,e. Classification is done to see whether different climate variations in tropics and extra-tropics exist. Therefore, the present study is focusing on the identification of possible sources of variability in large-scale circulation, and the dissimilarity between regions, rather than relationships among them. Results showed in the next section support this choice. The climate classification based on the monthly mean surface air temperature of two trimesters is described. Relationships with the large-scale circulation are explored through the calculation of correlation between the time series of each region (Figure 1c,e) and different climate fields. While correlation does not infer causality, it is a good indicator of covariability, providing some insight of potential teleconnection pathways.

3 | BOREAL WINTER

Applying the SOM to the surface air temperature bandpass filtered anomalies in DJF, eight regions are defined

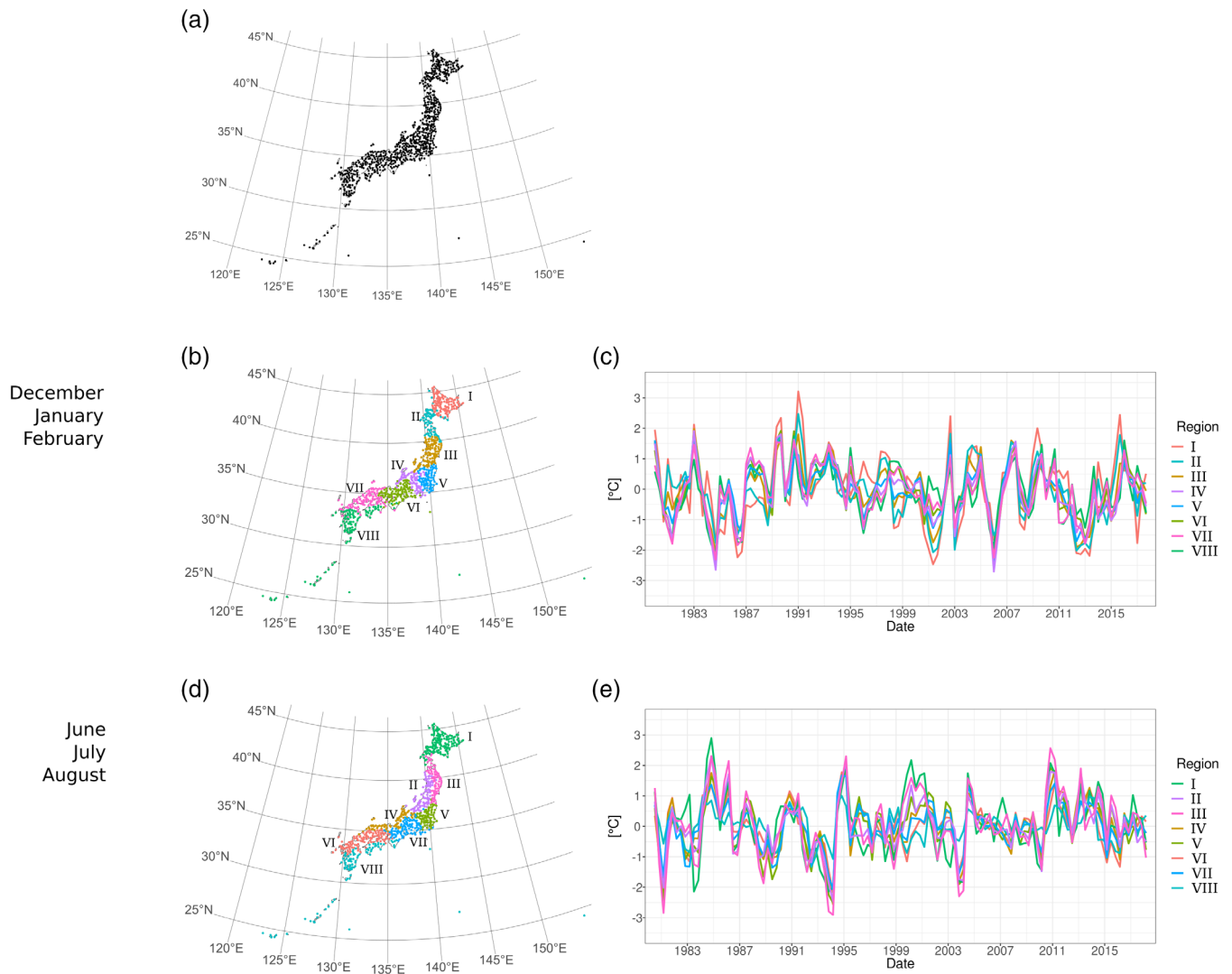


FIGURE 1 Spatial distribution of the 762 AMeDAS stations (a), eight regions from the classification for boreal winter (b), and associated time series (c). Eight regions from the classification for boreal summer (d) and associated time series (e)

(Figure 1b): Hokkaido (region I), northern part of Tohoku (region II), southern part of Tohoku and northern part of Hokuriku (region III), southern part of Hokuriku and Tokai (region IV), Kanto (region V), Tokai and Kinki (region VI), Chugoku, extreme northern Kyushu and northern Shikoku (region VII), and Kyushu, southern Shikoku and Okinawa (region VIII). The main direction of the divisions follows the north-south orientation, along with a secondary west-east orientation in the central part of the country. For each region, station SAT bandpass filtered anomalies are spatially averaged to construct an index (Figure 1c), subsequently used to calculate correlation coefficients with the monthly sea surface temperature (SST) bandpass filtered anomalies (Figure 2).

SAT index for Hokkaido (region I) is significantly and positively correlated ($+0.4 \sim +0.6$) with SST anomalies around Japan and in the vicinity of the Kuroshio extension (Figure 2a). Negative correlation coefficients ($-0.3 \sim -0.5$) are also found in the western Pacific, around 20°N . However, while it is the peak season of ENSO, there is no signal in the equatorial Pacific, suggesting an absence of clear influence of ENSO on the interannual variability of SAT in Hokkaido. Similar patterns are found with northern Tohoku (Figure 2b) but with weak positive correlation ($+0.1 \sim +0.3$) for the eastern equatorial Pacific. Compared with northern Tohoku, southern Tohoku has stronger relationship with the eastern Pacific (Figure 2c). The shape of positive correlations ($+0.3 \sim +0.5$) clearly resembles the eastern-Pacific El

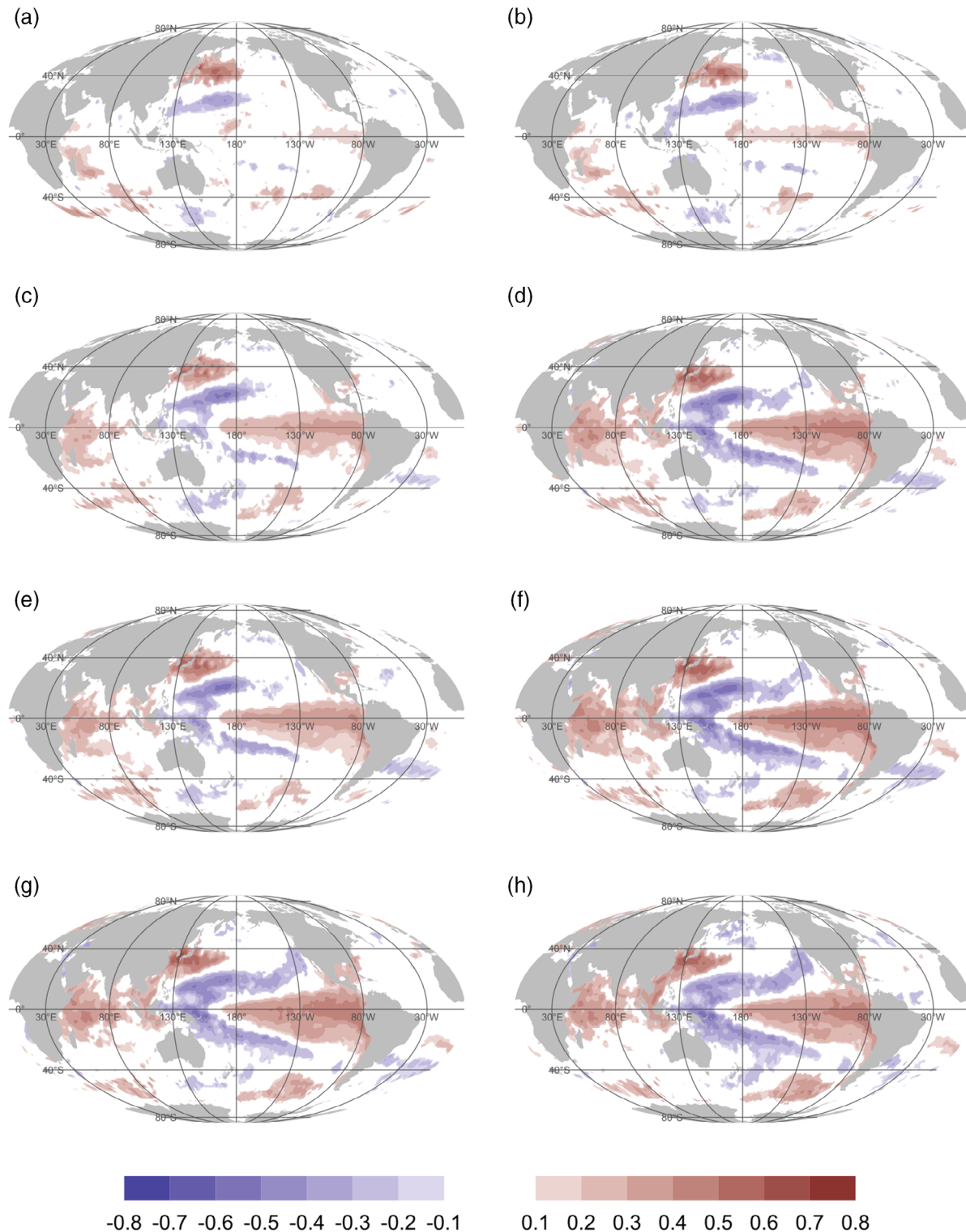


FIGURE 2 Correlation coefficients between DJF time series (Figure 1c) and the sea-surface temperature bandpass filtered anomalies. Only values significant at the 95% level (according to a Monte-Carlo resampling, $n = 10.000$) are displayed

Niño, with opposite correlations to the west mainly in the northern tropical Pacific ($-0.3 \sim -0.5$). This suggests that warmer (cooler) SAT anomalies in southern Tohoku are partly associated with the co-occurrence of an El

Niño (La Niña) event. Our results also suggest that Hokkaido and northern Tohoku should be considered as a whole and be separated from southern Tohoku, when exploring the relationships with ENSO. For regions south

of southern Tohoku, the signals in the tropical Pacific are further clear, indicating a horseshoe-shape pattern with negative correlations extending from the western tropical Pacific to the subtropical eastern North and South Pacific (Figure 2d–h). Interestingly, the signals in the tropics is slightly weaker for the region V compared to those for the regions IV and VI. These suggest that the influence from ENSO on SAT of respective regions could gradually increase towards the southwestern parts of the country. Related to those regions, positive correlation pattern is also seen in the western tropical Indian Ocean, but it is again slightly weaker for the region V than that for the regions IV and VI. The correlation pattern near Japan is likely to be the result of remote forcing and not the source of SAT variability, as it progresses from north to south according to the geographical distribution of the divisions.

In Figure 2, a gradual change in the pattern of correlations with SST is clearly visible from region I to region VIII. To see the details of the teleconnection patterns for the whole eight regions, we select three typical regions we analyse in the following sub-sections.

3.1 | Hokkaido: Cloud cover and southerly wind anomalies

Warmer SAT anomalies in Hokkaido (region I) have positive correlation with OLR over Japan, Japan Sea and eastern China (OLR, Figure 3). While this suggests an importance of the shortwave radiation, our detailed analyses showed that shortwave radiation has negative correlation with the SAT anomalies (not shown). This counterintuitive relationship implies that the warm SAT anomalies over Hokkaido are associated with increased low-level clouds. Also, anomalies of both latent and sensible heat fluxes seem to be an effect of warm SAT. These imply that probably anomalous anticyclonic circulation over North Pacific, with southerly wind anomalies in the lower troposphere above Japan (V 850 hPa, Figure 3), help to weaken cold northerlies and induce the warm SAT anomalies. In upper troposphere, easterly wind anomalies exist around 40°N (U 500 and 300 hPa, Figure 3), north to the average position of the subtropical jet in winter (30°N), suggesting a northward shift of the westerly jet. Together with the eastward wind anomalies over western Siberia, the pattern resembles the projection of the negative phase of the West Pacific (WP) pattern (Wallace and Gutzler, 1981; Barnston and Livezey, 1987) on to the zonal wind. However, the correlation between the SAT index in this region and the bandpass filtered WP index is found to be very low ($r = -0.036$, $p = .700$), making it difficult to establish a direct link between them.

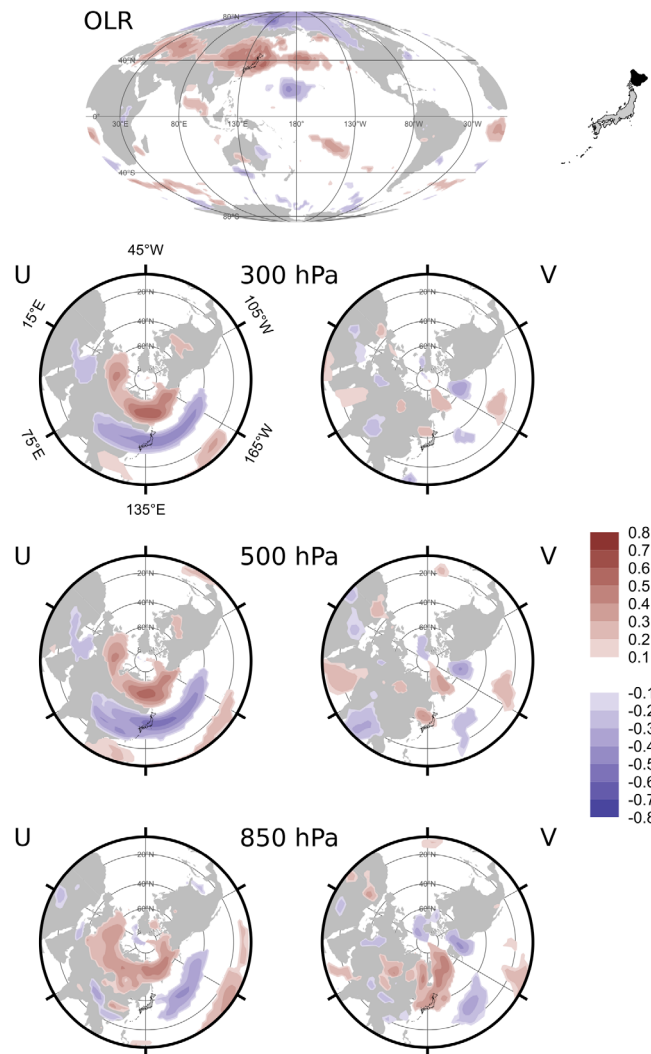


FIGURE 3 Correlation coefficients between DJF time series of region I (Figure 1c) and bandpass filtered anomalies of outgoing longwave radiation (OLR), zonal (U), and meridional (V) winds at 850, 500, and 300 hPa. Only values significant at the 95% level (according to a Monte-Carlo resampling, $n = 10.000$) are displayed

3.2 | Kanto region: The role of the subtropical westerly jet

In the Kanto region (region V), SAT anomalies are also linked to the cloud cover over Japan (OLR, Figure 4), cooler (warmer) being associated with enhanced (suppressed) cloudiness. The typical response of the OLR to the ENSO forcing (Liebmann and Hartmann, 1982; Deser and Wallace, 1990) is also visible in the tropics, over Eastern Africa, Maritime Continent and central Pacific Ocean. In lower troposphere, southerly wind anomalies (V 850 hPa, Figure 4) are associated with easterly wind anomalies around 25°N and westerly wind anomalies around 50°N (U 850 hPa, Figure 4). This again

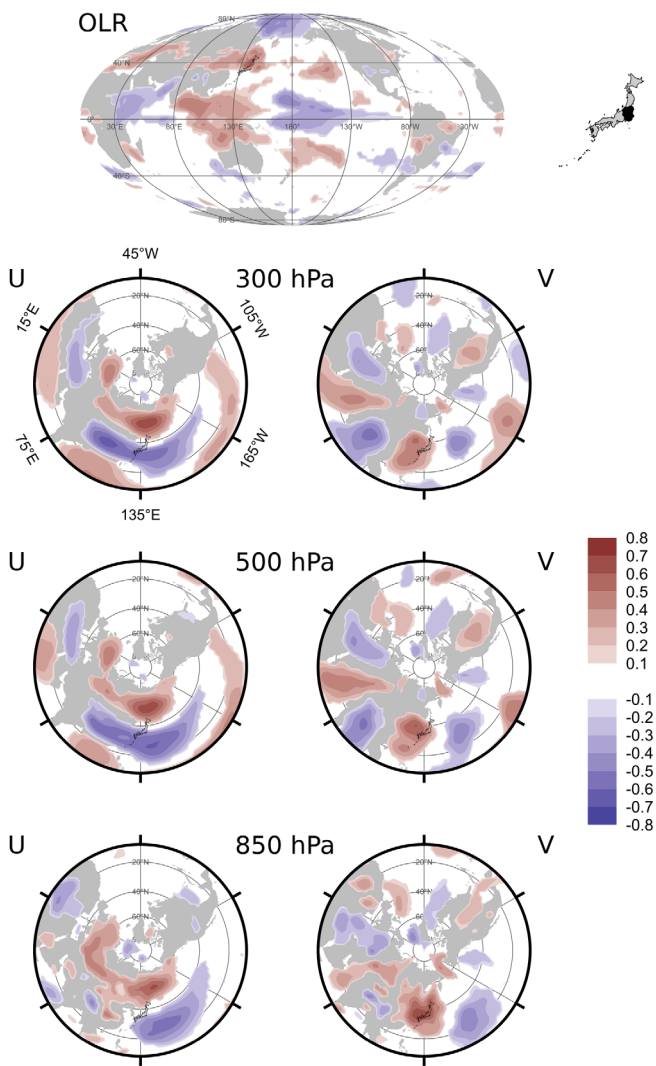


FIGURE 4 Correlation coefficients between DJF time series of region V (Figure 1c) and bandpass filtered anomalies of outgoing longwave radiation (OLR), zonal (U), and meridional (V) winds at 850, 500, and 300 hPa. Only values significant at the 95% level (according to a Monte Carlo resampling, $n = 10,000$) are displayed

suggests an anomalous anticyclonic circulation over the North Pacific, bringing warm air into the region. In upper troposphere, results suggest that when the subtropical westerly jet gets weaker, the Kanto region would be warmer (U 500 and 300 hPa, Figure 4). A WP-like pattern can also be found in the spatial correlation coefficients. The correlation between the region's SAT index and the WP index was stronger and significant ($r = -0.390$, $p < .01$) compared to their northern counterparts discussed earlier. Correlations with the meridional wind anomalies (V 500 and 300 hPa, Figure 4) depict a clear wave-like pattern, connecting the North Atlantic to the East Asia, similar to the Eurasian (EU) pattern (Wallace and Gutzler, 1981). The correlation between the region's

SAT index and the EU index is also strong ($r = -0.430$, $p < .01$). It is worth noting that the correlation between the WP and EU indices is low ($r = 0.243$, $p < .01$), limiting the risk of spurious association.

3.3 | Kyushu and Okinawa: Thermal advection and teleconnection patterns

Very similar results to those for the Kanto are found for the Kyushu/Okinawa (region VIII), albeit with a remarkable difference in OLR (Figure 5). While the signals in the tropics further clearly show the ENSO relating pattern, there is no clear signal with OLR over Japan, suggesting SAT variability is mainly a function of the advection of warm air from the tropics rather than higher amount of solar radiation. The signals in the middle and upper troposphere also become clearer especially in the wave-like pattern. The covariabilities with the WP and EU indices appear very strong here, with coefficients of -0.640 ($p < .01$) and -0.610 ($p < .01$), respectively.

4 | BOREAL SUMMER

From the SAT bandpass filtered anomalies in JJA, eight regions are defined through the SOM (Figure 1d). Except for Hokkaido (Region I), the north–south axis is the main separator. On the Sea of Japan side, western Tohoku/northern Hokuriku (Region II), southern Hokuriku/northern Kinki/northern Chugoku (Region IV) and southern Chugoku/northern Shikoku/northern Kyushu (Region VI). On the Pacific Ocean side, eastern Tohoku (Region III), Kanto (Region V), Tokai/southern Kinki (Region VII), and southern Shikoku/southern Kyushu/Okinawa (Region VIII). A spatial average of station SAT anomalies is again used to construct a SAT index for each region (Figure 1e). Those indices are then used to calculate correlation coefficients with SST, OLR, and components of the horizontal wind at three different levels.

Positive correlation coefficients are found between the Hokkaido SAT index and the SST anomalies in the vicinity of Japan and in the Kuroshio extension (Figure 6a). At the same time, negative coefficients are seen in the eastern tropical Pacific Ocean (La Niña-like pattern; correlation with Niño 3 index is -0.250 , $p = .041$), as well as in the northern Indian Ocean, in Maritime Continent and to some extent in the South China Sea. Negative coefficients in the eastern tropical Pacific Ocean are also found in the correlation plots of the other region indices (Figure 6b–g; correlations with Niño 3 index are -0.036 , $p = .410$, and -0.280 , $p = .034$, respectively). In northwest Pacific, the signal in the vicinity of Japan remains

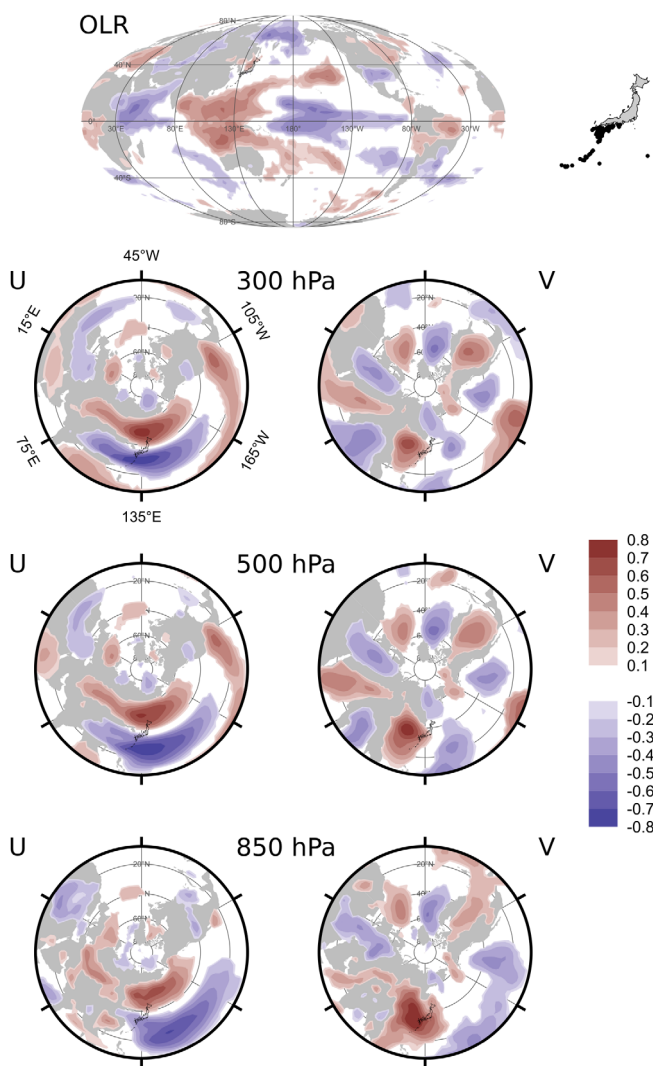


FIGURE 5 Correlation coefficients between DJF time series of region VIII (Figure 1c) and bandpass filtered anomalies of outgoing longwave radiation (OLR), zonal (U), and meridional (V) winds at 850, 500, and 300 hPa. Only values significant at the 95% level (according to a Monte-Carlo resampling, $n = 10.000$) are displayed

consistently positive through all the correlations plots of the different regions. However, negative coefficients in the South China Sea, while remain significant with SAT index of Tohoku regions (Figure 6b,c), disappear for other region indices (Figure 6d-h). The same inference is also drawn for the northern Indian Ocean. The SAT index of region VIII has some interesting signals in the tropical oceans. It is positively correlated with SST anomalies in the western Pacific Ocean, southeast of the South China Sea, where region I is negatively correlated. Also, negative correlations are found off the East African coast, location of the Western Pole of the Indian Ocean Dipole (IOD; Saji *et al.*, 1999). This could be the signs of the influence arising from the Indian Ocean during the formation of IOD, even though correlation coefficients with

IOD index are very low and not significant. As for DJF, representative regions are discussed below to see detailed relationships with large-scale atmospheric variability and its differences among the regions.

4.1 | Hokkaido: The role of the westerly jet stream

Pattern of correlation coefficients in the western Pacific Ocean at this time clearly resembles the Pacific-Japan (PJ) pattern (Nitta, 1987), with negative correlations over the Philippines and positive correlations over Japan (OLR, Figure 7). This confirms the influence of the PJ pattern on Japanese air temperature (Wakabayashi and Kawamura, 2004), with warmer (cooler) SAT anomalies in Hokkaido associated with positive (negative) PJ pattern. A pole of negative correlations is also located north of the PJ-like pattern, over the far east of Russia. This tripole looks similar to the pattern of correlations between PC1 of 850 hPa vorticity and surface air temperature (pattern of negative correlations over Philippines and Siberia, pattern of positive correlations over Japan) presented in Kubota *et al.* (2016), but with the Northernmost Pole shifted to the south. Similar shift of the Northern Pole can be also found in Kosaka *et al.* (2013). The correlation maps between the SAT index and the zonal wind (U at 850, 500 and 300 hPa, Figure 7) indicate the subtropical jet is weakened (negative correlation) compared to the mean state. In lower troposphere (V at 850 hPa, Figure 7), the pattern of correlations is not clear, but at 500 and 300 hPa, a wave train linking North Africa to western Pacific is also visible.

4.2 | Kanto region: Transition zone

Pattern of correlations between the Kanto region (region V) SAT index and the OLR are very similar (OLR, Figure 8) to the patterns found for Hokkaido region, that is, PJ-like pattern and Indian summer monsoon (ISM) signals. In the zonal wind, patterns are similar to those of region I (U at 850, 500 and 300 hPa, Figure 8). A pattern similar to the Silk Road pattern (Lu *et al.*, 2002; Enomoto *et al.*, 2003) is clearly found (V at 500 and 300 hPa, Figure 8) with a bifurcation around 105°E, creating a southern path (35°N) and a northern path (60°N) over eastern Asian and northwest Pacific.

4.3 | Kyushu and Okinawa: Influence of wave trains

Region VIII (southern Shikoku/southern Kyushu/Okinawa) correlations also clearly show the PJ pattern and

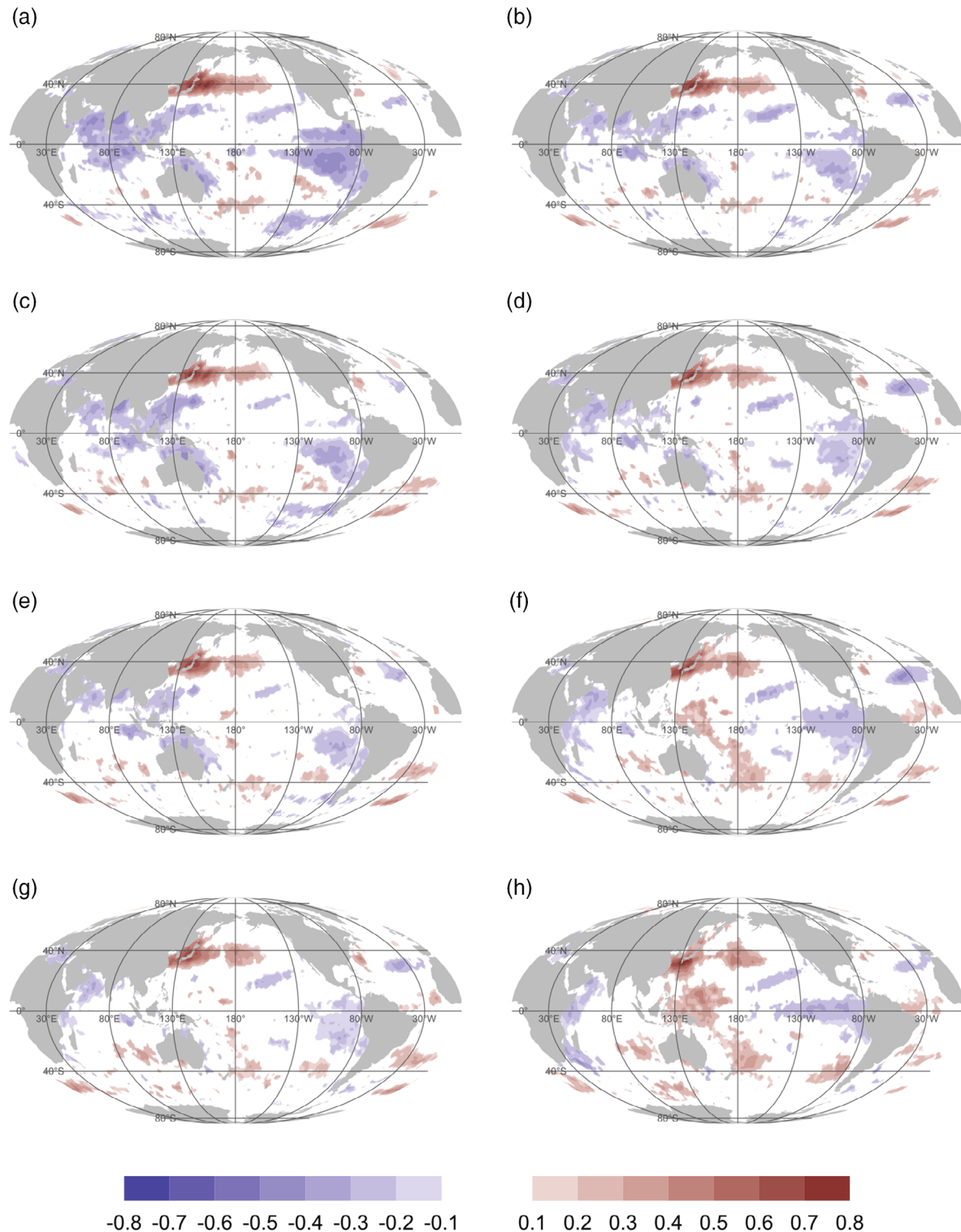


FIGURE 6 Correlation coefficients between JJA time series (Figure 1e) and the sea-surface temperature bandpass filtered anomalies. Only values significant at the 95% level (according to a Monte-Carlo resampling, $n = 10.000$) are displayed

the signal in the ISM region (OLR, Figure 9), while the third pole visible for Hokkaido and Kanto regions is not visible here. In the upper troposphere (500 and 300 hPa), the wave train linking North Africa to western Pacific,

with its bifurcation, remains an important feature of the anomalous circulation (500 and 300 hPa V, Figure 9).

In boreal summer, a strong symmetry exists between OLR and horizontal wind anomalies (Figures 7–9). Large

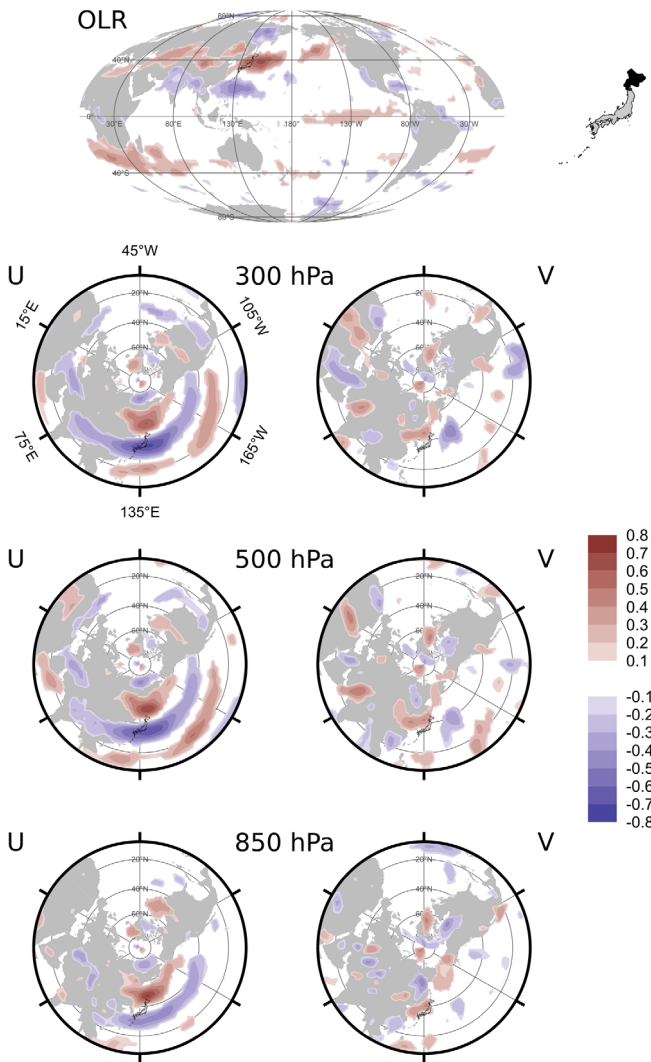


FIGURE 7 Correlation coefficients between JJA time series of region I (Figure 1e) and bandpass filtered anomalies of outgoing longwave radiation (OLR), zonal (U), and meridional (V) winds at 850, 500, and 300 hPa. Only values significant at the 95% level (according to a Monte-Carlo resampling, $n = 10.000$) are displayed

positive correlations in the former correspond to the region where the upper tropospheric jet anomalously slows down (negative correlation in zonal wind). Interestingly, the location of the symmetry in OLR and wind is moving: from region I to region VIII, the Northern Pole of the PJ-like pattern in the OLR shifts southward, followed by a similar shift in the westerly jet. Also, modulation, in speed and location, of the westerly jet seems to be the most important factor in explaining the variability of SAT in region I, when wave trains are most important in region VIII. Region V then appears as a transition zone, under the influence of both westerly jet and wave trains variations.

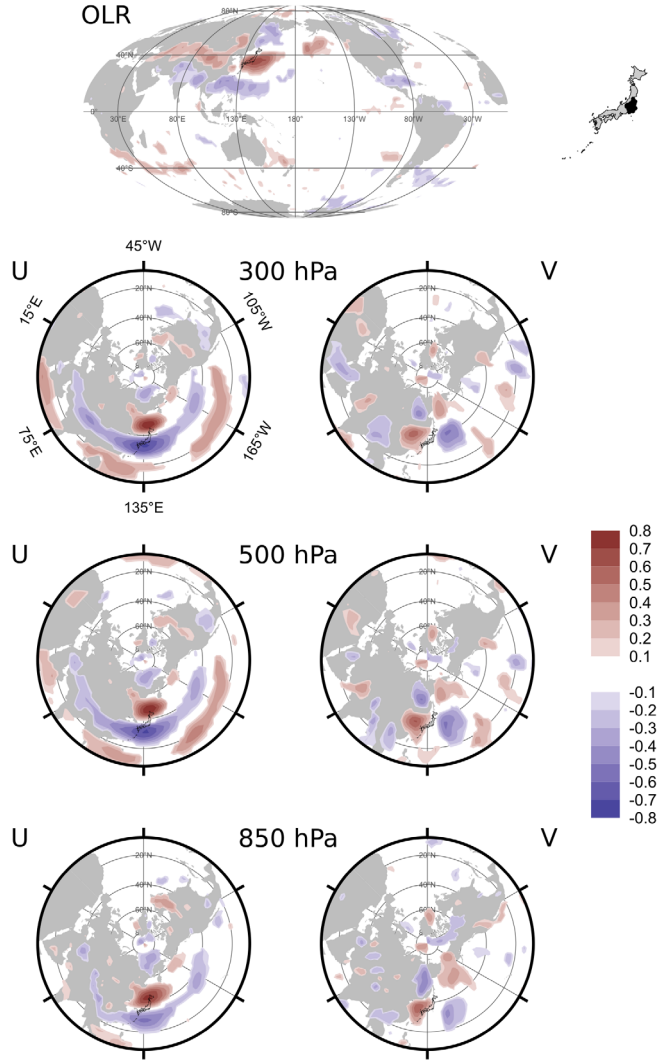


FIGURE 8 Correlation coefficients between JJA time series of region V (Figure 1e) and bandpass filtered anomalies of outgoing longwave radiation (OLR), zonal (U), and meridional (V) winds at 850, 500, and 300 hPa. Only values significant at the 95% level (according to a Monte-Carlo resampling, $n = 10.000$) are displayed

5 | DISCUSSION

5.1 | Boreal winter

It is found that the geographical distribution of classified regions is largely a function of the strength of the link with the tropical Pacific and Indian Oceans in this season; no link is found with the northern regions. In an earlier study, Shiozaki *et al.* (2017) also found none to very small temperature anomalies in Hokkaido during typical El Niño events (figure 1 in Shiozaki *et al.*, 2017), supporting our results. Southern regions have stronger link with tropical oceans, particularly ENSO in the Pacific Ocean and what resembles the Indian Ocean

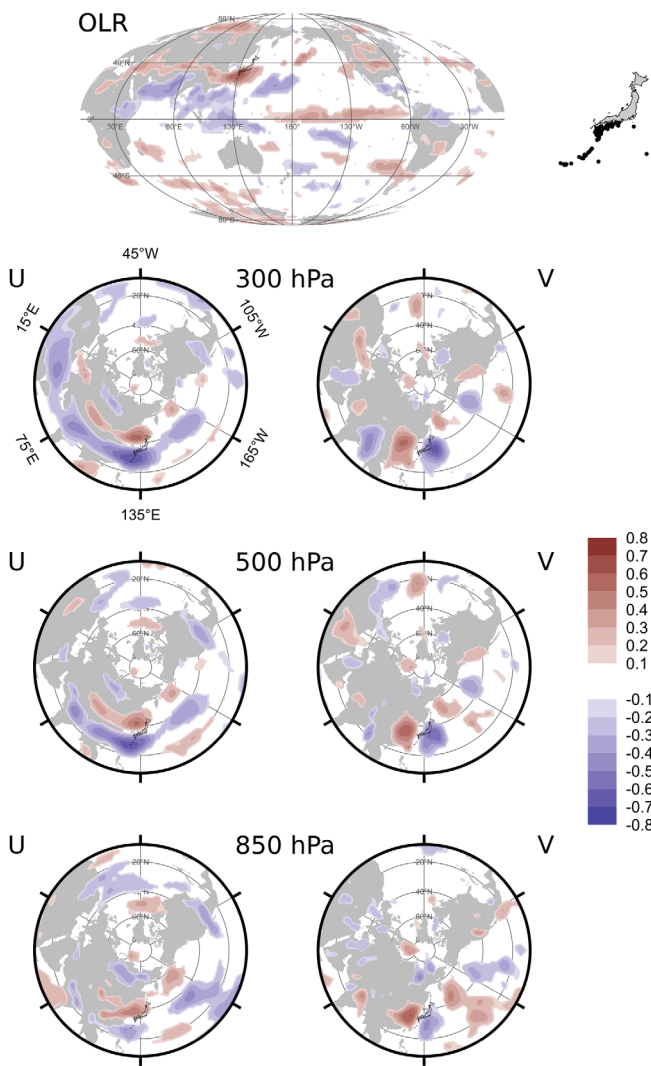


FIGURE 9 Correlation coefficients between JJA time series of region VIII (Figure 1e) and bandpass filtered anomalies of outgoing longwave radiation (OLR), zonal (U), and meridional (V) winds at 850, 500, and 300 hPa. Only values significant at the 95% level (according to a Monte-Carlo resampling, $n = 10.000$) are displayed

basin mode (Yulaeva and Wallace, 1994; Klein *et al.*, 1999). Detecting the development of such phenomena in advance (i.e., with the help of coupled models) would help to infer SAT amplitudes in southern regions.

The WP pattern is known to modulate the East Asian winter monsoon (Takaya and Nakamura, 2005a, 2005b, 2013) and the surface temperature in eastern Asia (Takaya and Nakamura, 2013; Oshika *et al.*, 2015; Tanaka *et al.*, 2016). The existence of a WP-like pattern in the correlations is consistent with figure 6 in Takaya and Nakamura (2013), who found that warmer 850-hPa temperature anomalies in January appear over most of Japan during a negative phase of WP-like pattern, together with an El Niño signal in the SSTs of the Pacific

Ocean. Interestingly, the variability of SAT anomalies in Japan is also a function of the link with the WP-like pattern, only strong and significant to the south, but very weak to the north. While the concurrence of WP pattern and ENSO seems important for SAT variability in boreal winter, the relationship between both is not necessarily strong (Kodera, 1998; Li and Wettstein, 2012; Tanaka *et al.*, 2016).

Also, from north to south, the influence of EU-like pattern strengthens, together with a stronger reduction of the speed of the westerly jet and a change in its location. Following the same path, the importance of the cloud cover over Japan weakens.

5.2 | Boreal summer

The PJ-like pattern is clearly visible for all regions and consistent with its known impact on the summer temperatures in Japan in recent decades (Wakabayashi and Kawamura, 2004; Kubota *et al.*, 2016), together with the western Pacific subtropical high shifting northward (Kubota *et al.*, 2016). But while PJ-like pattern is similar, its location is slightly different between selected regions and SST anomalies in tropical oceans. For northern regions of Japan, the SAT indices have negative correlations with the SSTs of the tropical Indian Ocean/South China Sea on the one hand and in eastern tropical Pacific on the other hand. This pattern is very similar to the map of regressed SST anomalies with respect to the PJ pattern index during the last decades (figures 4c and 8h in Kubota *et al.*, 2016). However, as the concurrences are moved from the north to the south, the link with Indian Ocean SST anomalies almost vanishes, while the sign of the correlations in the South China Sea reverses. At this time, the signal, though remains, has considerably reduced in the Pacific Ocean.

The Silk Road (SR) pattern (Lu *et al.*, 2002; Enomoto *et al.*, 2003), a wave train developing along the Asian jet, and a portion of the summertime circumglobal teleconnection (Branstator, 2002; Ding and Wang, 2005; Behera *et al.*, 2013), is also an important feature to explain the interannual variability of SAT in Japan. SR variability is known to be associated with heat waves in Japan, especially in August, through the reinforcement of the Bonin high (Enomoto, 2004), a subtropical anticyclone that is predominant near Japan in the summer (Enomoto *et al.*, 2003). The SR is generally associated with stronger convection over northwest India, which generates baroclinic circulation, a basic waveguide favourable to eastward-propagating Rossby waves (Enomoto *et al.*, 2003; Ding and Wang, 2005). In Figure 7, the SAT index of region I (Hokkaido) is negatively

correlated with OLR over India, implying SAT in Hokkaido are warmer when the ISM rainfall is above normal, through a more active SR. The signal in the JJA SST in the Indian Ocean-West Pacific sector is similar to the signal found by Kosaka *et al.* (2013) and is related to the ENSO during the previous winter, consistent with the signal found in Figure 6.

5.3 | Novelty of the approach

The classification of climate in Japan performed here differs from the “static” that is, not a function of the season, divisions of previous classifications. Results of the present study suggest that the climate division should depend on the considered season, because the link to the large-scale circulation and the SSTs evolve throughout the year. Previous studies have suggested different classifications. We find out that those are not useful for our purpose, because of their general consideration of time (interannual) and the space (regional) scales. For example, in boreal winter, Hokkaido and Tohoku are considered as one unique entity (Koizumi and Kato, 2012; Tanaka *et al.*, 2015); in a sense that colder or normal temperature is expected in northern Japan during El Niño events (Tanaka *et al.*, 2015). But this study shows a weak influence of ENSO in Hokkaido, compared to a much stronger influence in the Tohoku region. This suggests both regions should be considered as two distinct entities in boreal winter. On the other hand, some previous classification divides Hokkaido in sub-regions (e.g., Fukui, 1933; Isozaki, 1933; Sekiguchi, 1959; Suzuki, 1962; Yoshino, 1980), which appears exaggerated regarding the teleconnections found in this study. Another example with southern Kyushu and Okinawa could be considered as a single entity with this study, because of the similitude in their teleconnections, though these regions are considered separately, Okinawa/Amami on one hand, western Japan on the other hand (e.g., Fukui, 1933; Isozaki, 1933; Yoshino, 1980; Tanaka *et al.*, 2015).

Resulting division for the same geographical region can differ between DJF and JJA. For example, in case of the Tohoku (northern Japan) index, one signal is apparent in DJF but two signals in JJA while trying to link the global SST anomalies. In summer, the east–west difference could be due to the influence of the Yamase wind, a cold northeasterly wind which produces cool weather in summer over northeastern Japan (Ninomiya and Mizuno, 1985a, 1985b; Kanno, 1997), which sometimes has a huge impact on the rice harvest and the food policy (Kodama, 1997). The occurrence of the Yamase wind is strongly tied the activity of the Okhotsk high and can induce cool summers in northern Japan when it is more

frequent (Shimada *et al.*, 2014). The classification also shows some persistent regions between DJF and JJA, such as Hokkaido and Kanto, emphasizing their intrinsic uniqueness in regard to the interannual variability.

This is also a good indicator that the large-scale topography imprint in the SAT data is well captured by the classification, in the absence of local topography. During boreal summer, the east–west difference could be also explained by the interaction between the Yamase and the mountain ranges found in the central part of the region, emphasizing the ability of the SOM classification to capture the large-scale topography imprint. Regarding the Kanto plain, a flat region surrounded by mountainous area, this feature is clearly visible in the regionalization, both in winter and summer. It is worth noting that with a smaller number of nodes (<8), generally merged with another region (either southern Tohoku or central Japan), the Kanto plain is not well captured.

6 | CONCLUSION

We propose another approach to classify the climate of Japan using the self-organizing map applied on surface air temperature anomalies. Most importantly, the classification is seasonally stratified for two target seasons of boreal winter and summer in order to better capture specific seasonal signals while creating homogeneous regions.

Main inference from the study is that the SOM is able to create homogeneous regions solely using the interannual signal of SAT. Divisions created by the SOM show clear differences from north to south in boreal winter, from north to south (primary) and from west to east in northern Japan (secondary) in boreal summer. SOM is an objective method, easy to implement and able to detect inherent patterns in SAT, solely based on the differentiation of underlying physical process in action.

Other important findings are the distinct role of remote teleconnections on SAT interannual variability. In southern regions, strong relationships with tropics are found, particularly with sea surface temperature anomalies in both Indian and Pacific Oceans. In northern regions, extra-tropical atmospheric circulation exerts a stronger control on SAT variability at interannual time scale.

SAT index time series have their own interannual variability (Figure 1c,e), with very similar anomalies in some years but with also large difference in some other years. This study did not focus on the understanding of underlying processes for such a behaviour and it will be the main topic of another upcoming work. Also, the seasonal division of climate could be refined by introducing

other variables, such as precipitation (particularly if the interest is the rainy season in boreal spring and fall), minimum and maximum temperature for example, and by using a multivariate SOM.

ACKNOWLEDGEMENTS

The research was partly supported by JERA Co., Inc. The authors would like to thank two anonymous reviewers for their helpful comments. The authors are also grateful to Japanese Meteorological Agency, Met Office Hadley Centre and NOAA/OAR/ESRL PSD for providing dataset.

ORCID

Pascal Oettli  <https://orcid.org/0000-0002-4654-0251>

REFERENCES

- Annas, S., Kanai, T. and Koyama, S. (2007) Principal component analysis and self-organizing map for visualizing and classifying fire risks in forest regions. *Agricultural Information Research*, 16(2), 44–51. <https://doi.org/10.3173/air.16.44>.
- Anyadike, R.N.C. (1987) A multivariate classification and regionalization of West African climates. *Journal of Climatology*, 7(2), 157–164. <https://doi.org/10.1002/joc.3370070206>.
- Astel, A., Tsakovski, S., Barbieri, P. and Simeonov, V. (2007) Comparison of self-organizing maps classification approach with cluster and principal components analysis for large environmental data sets. *Water Research*, 41(19), 4566–4578. <https://doi.org/10.1016/j.watres.2007.06.030>.
- Ayoade, J.O. (1976) On the use of multivariate techniques in climatic classification and regionalization. *Archiv für Meteorologie, Geophysik und Bioklimatologie Serie B*, 24(4), 257–267. <https://doi.org/10.1007/BF02263458>.
- Barnston, A.G. and Livezey, R.E. (1987) Classification, seasonality and persistence of low-frequency atmospheric circulation patterns. *Monthly Weather Review*, 115(6), 1083–1126. [https://doi.org/10.1175/1520-0493\(1987\)115<1083:CSAPOL>2.0.CO;2](https://doi.org/10.1175/1520-0493(1987)115<1083:CSAPOL>2.0.CO;2).
- Behera, S., Ratnam, J.V., Masumoto, Y. and Yamagata, T. (2013) Origin of extreme summers in Europe: the indo-Pacific connection. *Climate Dynamics*, 41(3–4), 663–676. <https://doi.org/10.1007/s00382-012-1524-8>.
- Behera, S.K., Rao, S.A., Saji, N.H. and Yamagata, T. (2003) Comments on “A cautionary note on the interpretation of EOFs”. *Journal of Climate*, 16(7), 1087–1093. [https://doi.org/10.1175/1520-0442\(2003\)016<1087:COACNO>2.0.CO;2](https://doi.org/10.1175/1520-0442(2003)016<1087:COACNO>2.0.CO;2).
- Björnsson, H. and Venegas, S.A. (1997) *A Manual for EOF and SVD Analyses of Climatic Data*. Montreal, Canada: McGill University, p. 52.
- Branstator, G. (2002) Circumglobal teleconnections, the jet stream waveguide, and the North Atlantic oscillation. *Journal of Climate*, 15(14), 1893–1910. [https://doi.org/10.1175/1520-0442\(2002\)015<1893:CTTJSW>2.0.CO;2](https://doi.org/10.1175/1520-0442(2002)015<1893:CTTJSW>2.0.CO;2).
- Cannon, A.J. (2012) Köppen versus the computer: comparing Köppen-Geiger and multivariate regression tree climate classifications in terms of climate homogeneity. *Hydrology and Earth System Sciences*, 16(1), 217–229. <https://doi.org/10.5194/hess-16-217-2012>.
- Chattpadhyay, R., Vintzileos, A. and Zhang, C. (2013) A description of the madden-Julian oscillation based on a self-organizing map. *Journal of Climate*, 26(5), 1716–1732. <https://doi.org/10.1175/JCLI-D-12-00123.1>.
- Deser, C. and Wallace, J.M. (1990) Large-scale atmospheric circulation features of warm and cold episodes in the tropical Pacific. *Journal of Climate*, 3(11), 1254–1281. [https://doi.org/10.1175/1520-0442\(1990\)003<1254:LSACFO>2.0.CO;2](https://doi.org/10.1175/1520-0442(1990)003<1254:LSACFO>2.0.CO;2).
- Ding, Q. and Wang, B. (2005) Circumglobal teleconnection in the northern hemisphere summer. *Journal of Climate*, 18(17), 3483–3505. <https://doi.org/10.1175/JCLI3473.1>.
- Dommegård, D. and Latif, M. (2002) A cautionary note on the interpretation of EOFs. *Journal of Climate*, 15(2), 216–225. [https://doi.org/10.1175/1520-0442\(2002\)015<0216:ACNOTI>2.0.CO;2](https://doi.org/10.1175/1520-0442(2002)015<0216:ACNOTI>2.0.CO;2).
- Dommegård, D. and Latif, M. (2003) Comments on “A cautionary note on the interpretation of EOFs”—reply. *Journal of Climate*, 16(7), 1094–1097. [https://doi.org/10.1175/1520-0442\(2003\)016<1094:R>2.0.CO;2](https://doi.org/10.1175/1520-0442(2003)016<1094:R>2.0.CO;2).
- Enomoto, T. (2004) Interannual variability of the Bonin high associated with the propagation of Rossby waves along the Asian jet. *Journal of the Meteorological Society of Japan*, 82(4), 1019–1034. <https://doi.org/10.2151/jmsj.2004.1019>.
- Enomoto, T., Hoskins, B.J. and Matsuda, Y. (2003) The formation mechanism of the Bonin high in august. *Quarterly Journal of the Royal Meteorological Society*, 129(587), 157–178. <https://doi.org/10.1256/qj.01.211>.
- Forgy, E.W. (1965) Cluster analysis of multivariate data: efficiency versus interpretability of classification. *Biometrics*, 21(3), 768–769.
- Fukui, E. (1933) The climatic province of Japan (in Japanese). *Geographical Review of Japan*, 9(1–4), 1–19, 109–127, 195–219, 271–300.
- Fukui, E. (1938) *Climatology*. Tokyo, Japan: Kikon Shoin (in Japanese).
- Fukui, E. (1957) The second Thornthwaite climatic classification of Japan (in Japanese). *Tokyo Kyoiku Daigaku Chirigaku Kenkyuhokoku*, 1, 103–112.
- Geiger, R. (1954) *Classification of the Climate According to W. Köppen [in German]*. Landolt-Börnstein—Numerical Values and Functions for Physics, Chemistry, Astronomy, Geophysics, and Technology (in German). Berlin, Germany: Springer, pp. 603–607.
- Hannachi, A., Jolliffe, I.T., Stephenson, D.B. and Trendafilov, N. (2006) In search of simple structures in climate: simplifying EOFs. *International Journal of Climatology*, 26(1), 7–28. <https://doi.org/10.1002/joc.1243>.
- Hartigan, J.A. and Wong, M.A. (1979) Algorithm AS 136: a k-means clustering algorithm. *Journal of the Royal Statistical Society. Series C (Applied Statistics)*, 28(1), 100–108. <https://doi.org/10.2307/2346830>.
- Hewitson, B.C. and Crane, R.G. (2002) Self-organizing maps: applications to synoptic climatology. *Climate Research*, 22(1), 13–26. <https://doi.org/10.3354/cr022013>.
- Hotelling, H. (1936) Relations between two sets of variates. *Biometrika*, 28(3/4), 321–377. <https://doi.org/10.2307/2333955>.
- Hothorn, T., Hornik, K., van de Wiel, M.A. and Zeileis, A. (2006) A lego system for conditional inference. *The American Statistician*, 60(3), 257–263. <https://doi.org/10.1198/000313006X118430>.

- Hothorn, T., Hornik, K., van de, W.M. and Zeileis, A. (2008) Implementing a class of permutation tests: the coin package. *Journal of Statistical Software*, 28(1), 1–23. <https://doi.org/10.18637/jss.v028.i08>.
- Isozaki, M. (1933) The new Thornthwaite climatic classification and its adaptation to Japanese region (in Japanese). *Chigaku Zasshi*, 45(5), 234–245. <https://doi.org/10.5026/jgeography.45.234>.
- JMA. (2018) *Comments on Meteorological Observation Statistics (in Japanese)*. Tokyo, Japan: Japan Meteorological Agency, p. 126.
- Jolliffe, I.T. (2003) A cautionary note on artificial examples of EOFs. *Journal of Climate*, 16(7), 1084–1086. [https://doi.org/10.1175/1520-0442\(2003\)016<1084:ACNOAE>2.0.CO;2](https://doi.org/10.1175/1520-0442(2003)016<1084:ACNOAE>2.0.CO;2).
- Kanamitsu, M., Ebisuzaki, W., Woollen, J., Yang, S.-K., Hnilo, J.J., Fiorino, M. and Potter, G.L. (2002) NCEP–DOE AMIP-II reanalysis (R-2). *Bulletin of the American Meteorological Society*, 83(11), 1631–1643. <https://doi.org/10.1175/BAMS-83-11-1631>.
- Kanno, H. (1997) Classification of the Yamase (cold northeasterly wind around northeastern Japan) based upon its air-mass vertical structures. *Journal of the Meteorological Society of Japan. Ser. II*, 75(6), 1053–1071. https://doi.org/10.2151/jmsj1965.75.6_1053.
- Klein, S.A., Soden, B.J. and Lau, N.-C. (1999) Remote Sea surface temperature variations during ENSO: evidence for a tropical atmospheric bridge. *Journal of Climate*, 12(4), 917–932. [https://doi.org/10.1175/1520-0442\(1999\)012<0917:RSSTVD>2.0.CO;2](https://doi.org/10.1175/1520-0442(1999)012<0917:RSSTVD>2.0.CO;2).
- Kodama, Y.-M. (1997) Airmass transformation of the Yamase airflow in the summer of 1993. *Journal of the Meteorological Society of Japan. Ser. II*, 75(3), 737–751. https://doi.org/10.2151/jmsj1965.75.3_737.
- Kodera, K. (1998) Consideration of the origin of the different mid-latitude atmospheric responses among El Niño events. *Journal of the meteorological Society of Japan Ser. II*, 76(3), 347–361. https://doi.org/10.2151/jmsj1965.76.3_347.
- Kohonen, T. (1982) Self-organized formation of topologically correct feature maps. *Biological Cybernetics*, 43(1), 59–69. <https://doi.org/10.1007/BF00337288>.
- Kohonen, T. (2001) *Self-organizing maps*. Heidelberg, Berlin, Germany: Springer.
- Koizumi, K. and Kato, H. (2012) Climatic division of Japan depending on the spatial variation pattern of climatic elements (in Japanese). In: *Proceedings of the Institute of Natural Sciences*, Nihon University, Vol. 47, pp. 185–197.
- Kojima, C. (1973) Detailed climatic classification of Tohoku district by principal component analysis (in Japanese). *Journal of Agricultural Meteorology*, 29(3), 165–172. <https://doi.org/10.2480/agrmet.29.165>.
- Köppen, W.P. (1900) Attempted climate classification in relation to plant distributions (in German). *Geographische Zeitschrift*, 6, 593–611 & 657–679.
- Köppen, W.P. (1918) Classification of climates according to temperature, precipitation and seasonal cycle (in German). *Petermanns Geographische Mitteilungen*, 64, 193–203 & 243–248.
- Kosaka, Y., Xie, S.-P., Lau, N.-C. and Vecchi, G.A. (2013) Origin of seasonal predictability for summer climate over the Northwestern Pacific. *Proceedings of the National Academy of Sciences*, 110(19), 7574–7579. <https://doi.org/10.1073/pnas.1215582110>.
- Kottek, M., Grieser, J., Beck, C., Rudolf, B. and Rubel, F. (2006) World map of the Köppen-Geiger climate classification updated. *Meteorologische Zeitschrift*, 15(3), 259–263. <https://doi.org/10.1127/0941-2948/2006/0130>.
- Kubota, H., Kosaka, Y. and Xie, S.-P. (2016) A 117-year long index of the Pacific-Japan pattern with application to interdecadal variability. *International Journal of Climatology*, 36(4), 1575–1589. <https://doi.org/10.1002/joc.4441>.
- Langfelder, P. and Horvath, S. (2008) WGCNA: an R package for weighted correlation network analysis. *BMC Bioinformatics*, 9(1), 559. <https://doi.org/10.1186/1471-2105-9-559>.
- Langfelder, P. and Horvath, S. (2012) Fast R functions for robust correlations and hierarchical clustering. *Journal of Statistical Software*, 46(11), 1–17. <https://doi.org/10.18637/jss.v046.i11>.
- Lee, H.-T. and NOAA CDR Program. (2018) NOAA Climate Data Record (CDR) of Monthly Outgoing Longwave Radiation (OLR), Version 2.7. NOAA National Centers for Environmental Information. <https://doi.org/10.7289/v5w37tkd>.
- Leloup, J., Lachkar, Z., Boulanger, J.-P. and Thiria, S. (2007) Detecting decadal changes in ENSO using neural networks. *Climate Dynamics*, 28(2–3), 147–162. <https://doi.org/10.1007/s00382-006-0173-1>.
- Leloup, J., Lengaigne, M. and Boulanger, J.-P. (2008) Twentieth century ENSO characteristics in the IPCC database. *Climate Dynamics*, 30(2–3), 277–291. <https://doi.org/10.1007/s00382-007-0284-3>.
- Li, C. and Wettstein, J.J. (2012) Thermally driven and eddy-driven jet variability in reanalysis. *Journal of Climate*, 25(5), 1587–1596. <https://doi.org/10.1175/JCLI-D-11-00145.1>.
- Liebmann, B. and Hartmann, D.L. (1982) Interannual variations of outgoing IR associated with tropical circulation changes during 1974–78. *Journal of the Atmospheric Sciences*, 39(5), 1153–1162. [https://doi.org/10.1175/1520-0469\(1982\)039<1153:IVOOIA>2.0.CO;2](https://doi.org/10.1175/1520-0469(1982)039<1153:IVOOIA>2.0.CO;2).
- Liu, Y. and Weisberg, R.H. (2011) A review of self-organizing map applications in meteorology and oceanography. In: *Mwasiagi II (ed) Self Organizing Maps*. Rijeka, Croatia: IntechOpen, pp. 253–272.
- Liu, Y., Weisberg, R.H. and Mooers, C.N.K. (2006) Performance evaluation of the self-organizing map for feature extraction. *Journal of Geophysical Research*, 111(C5), C05018_1–C05018_14. <https://doi.org/10.1029/2005JC003117>.
- Lloyd, S. (1957) Least squares quantization in PCM. *IEEE Transactions on Information Theory*, 28(2), 129–137. <https://doi.org/10.1109/TIT.1982.1056489>.
- Lu, R.-Y., Oh, J.-H. and Kim, B.-J. (2002) A teleconnection pattern in upper-level meridional wind over the north African and Eurasian continent in summer. *Tellus A*, 54(1), 44–55. <https://doi.org/10.1034/j.1600-0870.2002.00248.x>.
- MacQueen, J. 1967 Some methods for classification and analysis of multivariate observations. In: Le Cam, L.M. and Neyman, J. (Eds). *Proceedings of the Fifth Berkeley Symposium on Mathematical Statistics and Probability. Paper Presented at the Fifth Berkeley Symposium on Mathematical Statistics and Probability*. pp. 281–297.
- McBoyle, G.R. (1971) Climatic classification of Australia by computer. *Australian Geographical Studies*, 9(1), 1–14. <https://doi.org/10.1111/j.1467-8470.1971.tb00239.x>.

- McBoyle, G.R. (1972) Factor analytic approach to a climatic classification of Europe. *Climatological Bulletin*, 12, 1–11.
- Mizukoshi, M. (1977) Climatic division and climatography of Japan. In: Fukui, E. (Ed.) *The Climate of Japan*. Tokyo, Japan, and Amsterdam, NY: Kodansha and Elsevier Scientific Pub. Co., pp. 225–270.
- Morioka, Y., Tozuka, T. and Yamagata, T. (2010) Climate variability in the southern Indian Ocean as revealed by self-organizing maps. *Climate Dynamics*, 35(6), 1059–1072. <https://doi.org/10.1007/s00382-010-0843-x>.
- Nakagawa, G. (1899) On the climate division of Japan. *Chigaku Zasshi*, 11(5), 347–354_1. (in Japanese). <https://doi.org/10.5026/jgeography.11.347>.
- Ninomiya, K. and Mizuno, H. (1985a) Anomalous cold spell in summer over northeastern Japan caused by northeasterly wind from polar maritime airmass: part 1. EOF analysis of temperature variation in relation to the large-scale situation causing the cold summer. *Journal of the Meteorological Society of Japan. Ser. II*, 63(5), 845–857. https://doi.org/10.2151/jmsj1965.63.5_845.
- Ninomiya, K. and Mizuno, H. (1985b) Anomalously cold spell in summer over northeastern Japan caused by northeasterly wind from polar maritime airmass: part 2. Structure of the northeasterly flow from polar maritime airmass. *Journal of the Meteorological Society of Japan. Ser. II*, 63(5), 859–871. https://doi.org/10.2151/jmsj1965.63.5_859.
- Nitta, T. (1987) Convective activities in the tropical western Pacific and their impact on the northern hemisphere summer circulation. *Journal of the Meteorological Society of Japan. Ser. II*, 65 (3), 373–390. https://doi.org/10.2151/jmsj1965.65.3_373.
- Oettli, P., Tozuka, T., Izumo, T., Engelbrecht, F.A. and Yamagata, T. (2014) The self-organizing map, a new approach to apprehend the madden–Julian oscillation influence on the intraseasonal variability of rainfall in the southern African region. *Climate Dynamics*, 43(5), 1557–1573. <https://doi.org/10.1007/s00382-013-1985-4>.
- Ohba, M., Kadokura, S., Nohara, D. and Toyoda, Y. (2016) Rainfall downscaling of weekly ensemble forecasts using self-organising maps. *Tellus A: Dynamic Meteorology and Oceanography*, 68(1), 29293. <https://doi.org/10.3402/tellusa.v68.29293>.
- Oliver, J.E. (2005) Climate classification. In: Oliver, J.E. (Ed.) *Encyclopedia of World Climatology*. The Netherlands: Springer, pp. 218–227.
- Oshika, M., Tachibana, Y. and Nakamura, T. (2015) Impact of the winter North Atlantic oscillation (NAO) on the Western Pacific (WP) pattern in the following winter through Arctic Sea ice and ENSO: part I—observational evidence. *Climate Dynamics*, 45(5), 1355–1366. <https://doi.org/10.1007/s00382-014-2384-1>.
- Pearson, K. (1901) On lines and planes of closest fit to systems of points in space. *The London, Edinburgh, and Dublin Philosophical Magazine and Journal of Science*, 2(11), 559–572. <https://doi.org/10.1080/14786440109462720>.
- Preisendorfer, R.W. (1988) *Principal Component Analyses in Meteorology and Oceanography*. Amsterdam, NY: Elsevier.
- Preston-Whyte, R.A. (1974) Climatic classification of South Africa: a multivariate approach. *South African Geographical Journal*, 56(1), 79–86. <https://doi.org/10.1080/03736245.1974.10559527>.
- R Core Team. (2018) *R: A Language and Environment for Statistical Computing*. Vienna, Austria: R Foundation for Statistical Computing.
- Rayner, N.A., Parker, D.E., Horton, E.B., Folland, C.K., Alexander, L.V., Rowell, D.P., Kent, E.C. and Kaplan, A. (2003) Global analyses of sea surface temperature, sea ice, and night marine air temperature since the late nineteenth century. *Journal of Geophysical Research: Atmospheres*, 108(D14), 4407. <https://doi.org/10.1029/2002JD002670>.
- Reusch, D.B., Alley, R.B. and Hewitson, B.C. (2005) Relative performance of self-organizing maps and principal component analysis in pattern extraction from synthetic climatological data. *Polar Geography*, 29(3), 188–212. <https://doi.org/10.1080/789610199>.
- Saji, N.H., Goswami, B.N., Vinayachandran, P.N. and Yamagata, T. (1999) A dipole mode in the tropical Indian Ocean. *Nature*, 401 (6751), 360–363. <https://doi.org/10.1038/43854>.
- Sekiguchi, T. (1949) The Köppen climatic classification of Japan (in Japanese). *Shakai Chiri*, 15, 12–16.
- Sekiguchi, T. (1959) Climatic regions in Japan [in Japanese]. *Tokyo Kyoiku Daigaku Chirigaku Kenkyuhokoku*, 3, 65–78.
- Shimada, T., Sawada, M. and Iwasaki, T. (2014) Indices of cool summer climate in northern Japan: Yamase indices. *Journal of the Meteorological Society of Japan. Ser. II*, 92(1), 17–35. <https://doi.org/10.2151/jmsj.2014-102>.
- Shiozaki, M., Enomoto, T. and Takaya, K. (2017) Tropical Sea surface temperature anomaly and the winter climate of Japan during ENSO. *Disaster Prevention Research Institute Annuals*, 60, 486–490 (in Japanese).
- Steiner, D. (1960) A multivariate statistical approach to climatic regionalization and classification. *East African Agricultural and Forestry Journal*, 50(2), 329–347.
- Strasser, H. and Weber, C. (1999) On the asymptotic theory of permutation statistics. *Mathematical Methods of Statistics*, 8, 220–250.
- Suzuki, H. (1962) The classification of Japanese climates (in Japanese). *Geographical Review of Japan*, 35(5), 205–211. <https://doi.org/10.4157/grj.35.205>.
- Takaya, K. and Nakamura, H. (2005a) Geographical dependence of upper-level blocking formation associated with intraseasonal amplification of the Siberian high. *Journal of the Atmospheric Sciences*, 62(12), 4441–4449. <https://doi.org/10.1175/JAS3628.1>.
- Takaya, K. and Nakamura, H. (2005b) Mechanisms of intraseasonal amplification of the cold Siberian high. *Journal of the Atmospheric Sciences*, 62(12), 4423–4440. <https://doi.org/10.1175/JAS3629.1>.
- Takaya, K. and Nakamura, H. (2013) Interannual variability of the east Asian winter monsoon and related modulations of the planetary waves. *Journal of Climate*, 26(23), 9445–9461. <https://doi.org/10.1175/JCLI-D-12-00842.1>.
- Tanaka, M., Takekawa, M. and Notsuhara, S. (2015) Characteristics of the weather in Japan during El Niño/La Niña events [in Japanese]. In: *Ensemble Prediction System Update – El Niño/La Niña and Weather of Japan [in Japanese]*. Tokyo, Japan: Japan Meteorological Agency, pp. 152–163.
- Tanaka, S., Nishii, K. and Nakamura, H. (2016) Vertical structure and energetics of the western Pacific teleconnection pattern. *Journal of Climate*, 29(18), 6597–6616. <https://doi.org/10.1175/JCLI-D-15-0549.1>.

- Thornthwaite, C.W. (1931) The climates of North America: according to a new classification. *Geographical Review*, 21(4), 633–655. <https://doi.org/10.2307/209372>.
- Thornthwaite, C.W. (1943) Problems in the classification of climates. *Geographical Review*, 33(2), 233–255. <https://doi.org/10.2307/209776>.
- Thornthwaite, C.W. (1948) An approach toward a rational classification of climate. *Geographical Review*, 38(1), 55–94. <https://doi.org/10.2307/210739>.
- Torrence, C. and Compo, G.P. (1998) A practical guide to wavelet analysis. *Bulletin of the American Meteorological Society*, 79(1), 61–78. [https://doi.org/10.1175/1520-0477\(1998\)079<0061:APGTWA>2.0.CO;2](https://doi.org/10.1175/1520-0477(1998)079<0061:APGTWA>2.0.CO;2).
- Tozuka, T., Luo, J.-J., Masson, S. and Yamagata, T. (2008) Tropical Indian Ocean variability revealed by self-organizing maps. *Climate Dynamics*, 31(2), 333–343. <https://doi.org/10.1007/s00382-007-0356-4>.
- Wakabayashi, S. and Kawamura, R. (2004) Extraction of major teleconnection patterns possibly associated with the anomalous summer climate in Japan. *Journal of the Meteorological Society of Japan*, 82(6), 1577–1588. <https://doi.org/10.2151/jmsj.82.1577>.
- Wallace, J.M. and Gutzler, D.S. (1981) Teleconnections in the geopotential height field during the northern hemisphere winter. *Monthly Weather Review*, 109(4), 784–812. [https://doi.org/10.1175/1520-0493\(1981\)109<0784:TITGHF>2.0.CO;2](https://doi.org/10.1175/1520-0493(1981)109<0784:TITGHF>2.0.CO;2).
- Wehrens, R. and Buydens, L.M.C. (2007) Self- and super-organizing maps in R : the kohonen package. *Journal of Statistical Software*, 21(5), 1–19. <https://doi.org/10.18637/jss.v021.i05>.
- Wehrens, R. and Kruisselbrink, J. (2018) Flexible self-organizing maps in kohonen 3.0. *Journal of Statistical Software*, 87(7), 1–18. <https://doi.org/10.18637/jss.v087.i07>.
- Wickham, H. (2016) *ggplot2: Elegant Graphics for Data Analysis*. Cham, Switzerland: Springer.
- Wilks, D.S. (2011) *Statistical Methods in the Atmospheric Sciences*. Amsterdam, The Netherlands; Boston, MA: Elsevier/Academic Press.
- Willmott, C.J. (1977) Toward a new climatic regionalization of the contiguous United States. In: ERDA and NOAA (Eds.) *Proceedings of the Second National Solar Radiation Data Workshop*. Huntsville, AL: Johnson Environmental and Energy Center, pp. D1–D11.
- Wolski, P., Jack, C., Tadross, M., van Aardenne, L. and Lennard, C. (2018) Interannual rainfall variability and SOM-based circulation classification. *Climate Dynamics*, 50(1), 479–492. <https://doi.org/10.1007/s00382-017-3621-1>.
- Yoshino, M. (1980) The climatic regions of Japan (die Klimaregionen Japans). *Erdkunde*, 34(2), 81–87.
- Yulaeva, E. and Wallace, J.M. (1994) The signature of ENSO in global temperature and precipitation fields derived from the microwave sounding unit. *Journal of Climate*, 7(11), 1719–1736. [https://doi.org/10.1175/1520-0442\(1994\)007<1719:TSOEIG>2.0.CO;2](https://doi.org/10.1175/1520-0442(1994)007<1719:TSOEIG>2.0.CO;2).
- Zscheischler, J., Mahecha, M.D. and Harmeling, S. (2012) Climate classifications: the value of unsupervised clustering. *Procedia Computer Science*, 9, 897–906. <https://doi.org/10.1016/j.procs.2012.04.096>.

How to cite this article: Oettli P, Nonaka M, Kuroki M, Koshiba H, Tokiya Y, Behera SK. Understanding global teleconnections to surface air temperatures in Japan based on a new climate classification. *Int J Climatol*. 2020;1–16. <https://doi.org/10.1002/joc.6754>